Field-induced pseudocrystalline ordering in concentrated ferrofluids

A. Wiedenmann,[1,*] A. Hoell,[1] M. Kammel,[1] and P. Boesecke[2]
[1]*Hahn-Meitner-Institut Berlin, Department SF3, Glienickerstrasse 100, D-14109 Berlin, Germany*
[2]*European Synchrotron Radiation Facilities (ESRF), BP 220, F-38043 Grenoble Cedex, France*
(Received 13 December 2002; published 17 September 2003)

Concentrated surfactant stabilized cobalt ferrofluids up to 6 vol % Co have been studied by small-angle scattering using polarized neutrons and synchrotron x rays. The combination of these techniques allowed the magnetic and nuclear form factors to be reliably separated from the structure factors. Above 1 vol % Co, inter particle interactions are induced by an applied external magnetic field that gives rise to pseudocrystalline ordering of cobalt core-shell particles. Particles are arranged in hexagonal planes, with the magnetic moments aligned parallel to the [110] direction. Two types of equivalent textures were found to be present simultaneously, corresponding to a stacking of the hexagonal planes in horizontal and vertical direction. The in-plane nearest-neighbor distance is almost independent of the concentration and temperatures, whereas the distance between the neighboring planes, *c*, strongly varies from sample to sample. In addition, segments of chains of particles with parallel moments are aligned along the magnetic field and frozen-in when the carrier liquid is solidified. The field induced pseudocrystalline lamellar hexagonal particle arrangement, observed experimentally in colloidal magnetic liquids, confirms predictions from molecular-dynamics and Monte Carlo simulations.

DOI: 10.1103/PhysRevE.68.031203 PACS number(s): 61.12.Ex, 61.10.Eq, 75.50.Mm

I. INTRODUCTION

Ferrofluids (FF) are stable magnetic colloids in which nanoscaled magnetic particles are stabilized against coagulation either by electrostatic repulsion or by coating with organic chain molecules acting as surfactants [1,2]. Renewed interest of these materials is motivated by potential biomedical applications [3] based on the superparamagnetic behavior of nanosized particles, which disappears when aggregation takes place as a consequence of inefficient screening. We are currently performing a comprehensive investigation of density, concentration, and magnetization fluctuations of new FF by means of small-angle scattering (SAS) techniques. While x-ray scattering (SAXS) probes mainly the particle core (due to its high electron density), neutron scattering (SANS) gives access to the organic shell, the core, and the particle moments. Recently we demonstrated that small-angle scattering using polarized neutrons (SANSPOL) provide an additional contrast variation for the magnetic core [4–7] and allow the mesoscopic constituents of polydisperse FF to be identified quantitatively [8–12]. In very diluted Co ferrofluids, we were able to evaluate precisely the core-shell structure and size distribution of the nanoparticles. In more concentrated systems, the interaction potential should lead to correlations between particles defined by a correlation function $g(R)$, the Fourier transform of which is measured in scattering experiments as the so-called structure factor $S(Q)$. In magnetic colloids, the hard-core repulsion competes with van der Waals attraction and magnetic dipole-dipole interaction. As predicted by de Gennes and Pincus [13], the latter should give rise to a spontaneous arrangement of particles in chains or rings with magnetic moments parallel to each other. In an external magnetic field, these chains are expected to be aligned along the field direction that gives rise to anisotropic structure factors. The relative strength of the magnetic interaction, defined as the ratio between the dipole and thermal energy, is given by

$$\gamma = \frac{M_{sat}^2 V_c^2 \mu_0}{4\pi k_B T \sigma^3}, \tag{1}$$

where M_{sat} is the saturation magnetization of the particle with a core volume $V_c = \frac{4}{3}\pi R_c^3$ and $\sigma = 2(R_c + d)$ is the nearest distance between neighboring composite particles with a shell thickness d. Due to the long-range nature of the repulsive interaction between the induced magnetic dipoles for large values of γ, liquid-solid transitions have been predicted from simulations. Ordered structures have been observed experimentally up to now only in dipolar systems with millimeter-sized particles [14,15], while the particle arrangement in nanosized FF is still controversial where isotropic network structures [16] and anisotropic concentration fluctuations [17,18] have been reported.

Extraction of anisotropic structure factors from the SAS signal in polydisperse multiphase systems is a complicated task for which a precise knowledge of the scattering of the individual noninteracting particles alone is needed. The latter can be measured in very diluted samples or obtained from modeling of the intensity at high values of Q. We combined SANS, SANSPOL, and synchrotron SAXS measurements on the same samples and analyzed the scattering in the two-dimensional (2D) detector plane. The different contrasts of these techniques should allow magnetic and nonmagnetic contributions to be separated and hence the anisotropic structure factors to be extracted reliably. Samples of different particle concentrations were investigated in variable external magnetic fields applied in different directions parallel and perpendicular to the incident neutron or photon beam.

*Electronic address: wiedenmann@hmi.de

II. SCATTERING CROSS SECTIONS

In polydisperse multiphase systems when different types of particles, j, of different shape $F_j(QR)$ and size distributions $N_j(R)$ are embedded in a homogeneous matrix, the intensity of the SAS signal is given by

$$I(Q)=\sum_j \int F_j^2(QR)N_j(R)S_j(Q)dR, \tag{2}$$

where $N_j(R)\,dR$ is the incremental number density of particles of type j in the radius interval between R and $R+dR$ [19]. $F_j(QR)=\Delta\eta V_p f(QR)$ is the "form factor" of a particle with volume V_p, where $f(QR)$ depends only on the shape of the particle. $\Delta\eta$ is the contrast between scattering length densities of particle and matrix, i.e., $\Delta\eta=\eta_p-\eta_{matrix}$. For SANS the scattering length densities η are defined by

$$\eta_N=\sum \frac{c_j b_j}{\Omega_j},$$

$$\eta_M=\frac{e^2\gamma}{2mc^2}\sum \frac{c_j M_j^{\perp}}{\Omega_j} \tag{3}$$

for nuclear and magnetic scattering, respectively. b_j is the nuclear scattering length and $\mathbf{M}_\mathbf{j}^{\perp}$ is the projection of the magnetic moment onto a plane perpendicular to the scattering vector $\mathbf{Q}$ [with $|\mathbf{Q}|=(4\pi/\lambda)\sin\Theta$, where λ is the wavelength and 2Θ is the scattering angle]. c_j and Ω_j are the concentration and atomic volume of the species j, respectively. For SAXS, b_j has to be replaced in Eq. (3) by the complex atomic form factor $f_j(Q)$. Interparticle correlations are taken into account in Eq. (2) via the partial structure factors $S_j(\mathbf{Q})$ of all particles of type j. While analytical solutions are available only for monodisperse systems for the general case of Eq. (2), several approximations have been proposed [20–22]. A total structure factor $S(Q)$ is experimentally derived by dividing the measured scattering intensities by the normalized intensities of very diluted samples where $S(Q)$ is assumed to be unity and where only the form factors contribute to the scattering. Instead of the "very diluted" limit the intensities calculated from fits of the high-Q range can be used provided that the scattering contributions from form factors and the structure factor can be reliably separated.

For polarized neutrons where the neutron spins are aligned antiparallel $(+)$ or parallel $(-)$ to the magnetic-field vector $\mathbf{H}$, the scattering cross sections depend on the polarization P of the incident neutrons, respectively [23,24]. For the present case where the polarization of the scattered neutrons is not analyzed (denoted here as SANSPOL), the scattering intensities have been derived in Refs. [6–8] using the formalism presented in Refs. [24–26]. Depending on the polarization state of the incident neutrons, two different scattering signals are observed when magnetic particles are present. When single domain particles of saturation magnetization M_s^p are embedded in a nonmagnetic matrix, the two 2D SANSPOL cross sections $I^+(Q,\alpha)$ and $I^-(Q,\alpha)$ at a scattering vector Q, forming an angle α with the external magnetic field H, are derived as

$$I^{\mp}(Q,\alpha)=\{[F_M^2L^2(x)\pm 2F_MF_NL(x)]\sin^2\alpha+F_N^2\}$$
$$*S(Q,\alpha)+F_M^2\left[2\frac{L(x)}{x}-\sin^2\alpha\left(L^2(x)-1+3\frac{L(x)}{x}\right)\right], \tag{4}$$

where I^- refers to the positive sign in the first term of Eq. (4). In Eq. (4), nonperfect alignment of the superparamagnetic moments is taken into account by the Langevin statistics $L(x)=\coth(x)-(1/x)$, where $x=M(R)(H_{eff}/k_BT)$. The total particle moment, $M(R)=\frac{4}{3}\pi R^3 m_0\Omega$, depends on the radius R of the particles, where m_0 is the magnetic moment per atom. The intensities $I^+(Q,\alpha)$ and $I^-(Q,\alpha)$ are different for the two polarization states for any angle α except for $\alpha=0$, where the scattering vectors is parallel to $\mathbf{H}$ and where Eq. (4) simplifies to

$$I^{\pm}(Q\|H)=F_N^2S(Q\|H)+2F_M^2\frac{L(x)}{x}. \tag{5a}$$

While the first term results from nuclear correlations, the second term of Eq. (5a) is due to nonperfect alignment of the particle moment along $\mathbf{H}$ and vanishes in saturation where $(L(x)/x)=0$. The intensity difference between the two polarization states is given by

$$I^-(Q,\alpha)-I^+(Q,\alpha)=4F_NF_ML(x)S(Q,\alpha)\sin^2\alpha, \tag{5b}$$

which is linear in the nuclear and magnetic amplitudes. This cross term allows the structure factor $S(Q,\alpha)$ for any direction $\alpha>0$ to be precisely determined beside the field variation of the magnetic moment according to the Langevin statistics. Note that in Eq. (5a), interparticle correlations parallel to the field affect only the nuclear term, while correlations in all other directions influence nuclear, magnetic, and cross terms. As will be shown later, this feature of Eq. (5a) helps to distinguish between interparticle correlations and particular form factors, which both may give rise to characteristic peaks in the SANS curves at low Q.

III. EXPERIMENT

Samples of Co ferrofluids have been prepared by Berlin Heart AG applying decomposition of cobalt octacarbonyl using different types and concentrations of surfactants as stabilizers [27,28]. In a previous series of very low concentration, MF-56, pure oleoylsarcosine, $C_{21}-H_{39}-NO_3$, has been used as surfactant to coat the Co nanoparticles. In the series denoted as MF-239, beside $C_{21}-H_{39}-NO_3$, mixtures of two additional surfactants have been used in excess in order to prepare and stabilize the Co particles in fully deuterated toluene with nominal Co concentrations of about 1 vol % (D1) and 5 vol % (D5). In a second series, MF-254, a slightly different preparation technique has been applied resulting in larger Co particles (D3a and D5a). In a third series, MF-256, samples with nominal Co concentrations of 1%, 2%, 3%,

TABLE I. Co ferrofluids investigated by small-angle scattering and the resulting structural parameters: Average core radius $\langle R_{core}\rangle = \sqrt[3]{(1/N)\int N(R)R^3\,dR}$, shell thickness d, core volume fraction f and Q values are given, where intensity maxima occurred.

Sample (preparation)	H range (T)	Field direction with respect to neutron beam	SAS technique	$\langle R_{core}\rangle$ (nm)	d (nm)	f (vol %)	Positions of maxima Q_1	Q_2 (nm^{-1})	Q_3
(MF-239)									
D1	0–1	$H\perp n$	SANSPOL	3.75	2.3	0.6			
D5			SANSPOL	3.75	2.4	3.2	0.33		
(MF-254)									
D3a	0–00.3	$H\parallel n$	SANSPOL, 300 K	5.4	1.9	2.2			0.08
		$H\parallel n$	SANSPOL, 260 K						0.08
		$H\parallel n$	SANSPOL, 110 K						0.08
		$H\parallel n$	SANSPOL, 30 K						0.1
D3a	1	$H\perp n$	SANS, 300K	5.4	1.9	2.2	0.32		
D5a	3	$H\parallel n$	SANS			3.5			0.21
(MF-256)									
DS1	0–1	$H\perp n$	SANSPOL, SAXS	3.8	1.9	1			
DS2	0–1	$H\perp n$	SANSPOL, SAXS			2	0.34	0.57	0.26
	1	$H\perp n$	SANSPOL, 30 K				0.34		0.27
DS3	0–1	$H\perp n$	SANSPOL, SAXS			3	0.32	0.57	0.24
DS4	0–1	$H\perp n$	SANSPOL, SAXS			4	0.32	0.57	0.23
DS6	0–1	$H\perp n$	SANSPOL, SAXS			6	0.324	0.57	0.25

4%, and 6% (denoted as DS1 to DS6) have been prepared in toluene. The toluene carrier liquid was exchanged by deuterated toluene using dialysis technique. The preparation of Co cores by decomposition of cobalt octacarbonyl inside surfactant spheres yields particles with narrow size distribution. All samples were handled and sealed under argon gas and remained single-phase dispersions even under an applied field of up to 3 T. SANSPOL measurements were performed on the instrument $V4$ [4,5] installed at the BERII reactor of HMI, Berlin and SAXS experiments on the anomalous scattering beam-line ID01 at synchrotron ESRF in Grenoble, France. Samples of the series DS1-DS6 were placed in a horizontal magnetic field of strength up to 1.0 T, applied perpendicular to the incoming neutrons or x-ray photons. In addition, samples D3a and D5a were measured at different temperatures between 300 K and 30 K by SANSPOL when a magnetic field was applied parallel to the incoming neutron beam. Since sample specific differences were expected from the different preparation conditions, the structure parameters of all samples had to be evaluated by SANSPOL. The results are reported in Table I.

IV. RESULTS AND DISCUSSION

In previous studies of very diluted Co ferrofluids <0.5 vol % [6], we were able to evaluate precisely the core-shell structure of the nanoparticles by a simultaneous fit of the scattering curves $I^{\pm}(Q\perp H)$, F_M^2, and F_N^2. A sharp lognormal-type size distribution corresponding to a volume weighted average of the core radius of $\langle R'\rangle = 3.7$ nm and a constant thickness of the shell of $d=2.3$ nm was derived. The shell formed by the organic surfactant was found to be nearly impenetrable for the solvent. The magnetic moment of the core $M(H)$ follows a Langevin function as expected for superparamagnetic behavior of noninteracting single domain Co particles [7]. The same structural features were derived in case of the differently prepared samples D1 and D5 (Table I). An additional isotropic nonmagnetic scattering contribution is superimposed to I^+ and I^- at high Q corresponding to a small amount (1–5 vol %) of spherical particles with $R \approx 1.8$ nm, which might result from excess surfactant molecules still present in the solutions [9]. The difference curves $I^-(Q\perp H) - I^+(Q\perp H)$ have been fitted according to Eq. (5b) using a new algorithm described elsewhere [29,30]. Since all nonmagnetic contributions are canceled, the resulting structure parameters are obtained much more precisely using this technique. While for the diluted sample D1 no change of the particle arrangement is detected in an external field, in the concentrated sample D5 a pronounced peak occurs for both polarization states at $Q_1 = 0.32$ nm^{-1} when the magnetic field is turned on. In the first approach, we have analyzed the data in terms of a Percus-Yevick's model [20], corresponding to volume fraction $\eta = 0.3$ of hard spheres with a radius $R_{hc} = 8.65$ nm [9]. The same structure factor $S(Q)$ could be used in horizontal and vertical directions, which implied a rather dense packing of the particles. In order to clarify the nature of the field-induced correlations, we investigated carefully the whole 2D-scattering pattern as a function of the particle concentration, the strength, and the orientation of the applied magnetic field and of the temperature.

A. Concentration and field dependence

The two-dimensional SANS pattern for nonpolarized neutrons of samples of the series DS1-DS6 measured in a hori-

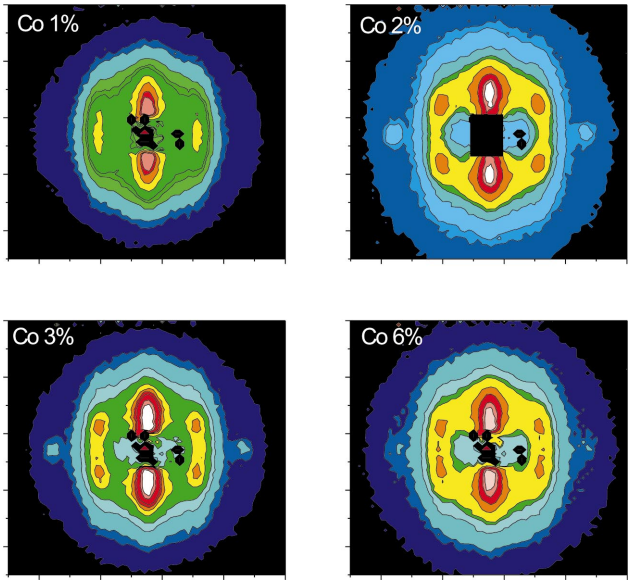

FIG. 1. (Color) 2D isointensity SANS pattern of Co-FF samples DS1, DS2, DS3, and DS6 for nonpolarized neutrons measured in a horizontal magnetic field of $H=1.1$ T, applied perpendicular to the incident neutrons.

zontal magnetic field of 1.1 T perpendicular to the incident beam is shown in Fig. 1. All samples with Co concentrations above 1 vol % exhibit pronounced peaks at low Q, which disappear in zero field. As a typical example, the 2D SANSPOL intensities I^- and I^+ for neutron spins parallel and antiparallel, respectively, are shown in Fig. 2 for the DS2 sample. The average $(I^-+I^+)/2$ corresponds to the scattering pattern of nonpolarized neutrons, while the difference pattern I^+-I^- of Fig. 2 reflects the nuclear-magnetic cross term resulting solely from magnetic particles. From Figs. 1 and 2, four peaks are clearly distinguished at scattering vectors with constant lengths corresponding to $Q_1=0.33$ nm^{-1} and forming angles of $\pm 30°$ with the horizontal direction of the applied magnetic field. Two additional peaks appear at $Q_2=0.57$ nm^{-1} in the horizontal direction.

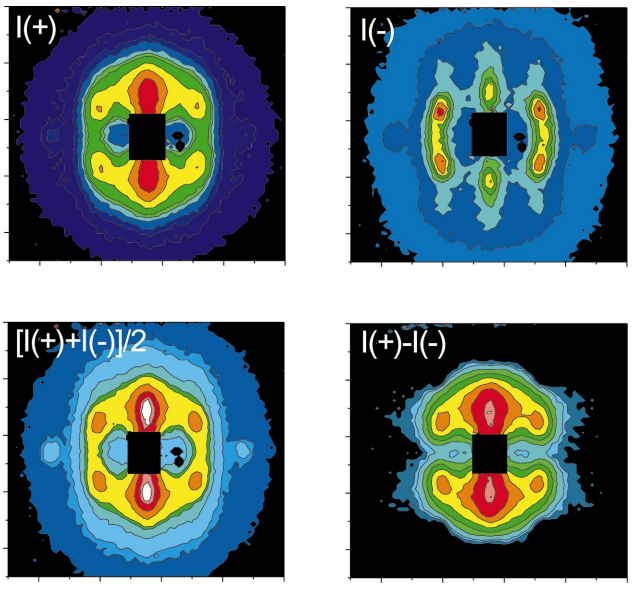

FIG. 2. (Color) 2D-SANSPOL intensities for 2 vol % Co-FF sample in horizontal magnetic field of 1 T with I^+ for neutron spin antiparallel to H and I^- for neutron spin parallel to H. The average $[I^++I^-]/2$ corresponds to the pattern of nonpolarized neutrons, and the difference pattern I^+-I^- represents the nuclear-magnetic cross term for one and the same particle. The interparticle correlation effect is clearly revealed in the appearance of pronounced peaks corresponding to hexagonal symmetry.

Figure 2 shows instructively how the different contrasts for I^+ and I^- or for nonpolarized neutrons affect the peaks differently: since reflections at Q_2 appear in directions parallel to H, their intensity must result from purely nuclear contrast and hence is equal for both neutron polarization states and disappears completely in the cross term. The 2D SANSPOL intensities I^+ and I^- were averaged over azimuth angles of $\Delta\alpha=10°$ and plotted in Fig. 3 for the sample with 3 vol % Co (DS3) for four sectors α. The scattering cross section in the high-Q part shows the characteristics of core-shell particles as observed in the diluted systems [6,8], i.e., crossover of the intensities $I^-(Q\perp H)$ and $I^+(Q\perp H)$ at $Q=0.7$ nm^{-1} and a shoulder around $Q=0.9$ nm^{-1}, which result from the form factors for polarized neutrons. While for the sector with $\alpha=30°$ the intensity is clearly peaked at Q_1 for both polarization states, the curve I^- for the sector at 60° is continuously increasing with decreasing Q, whereas I^+ still reveals a maximum at Q_2. In the horizontal sector with $\alpha=0°$ where the intensities were found to be independent of the neutron polarization, an additional peak is observed at Q_2. In the vertical sector ($\alpha=90°$) where the magnetic contribution is maximum, we find a strong and sharp peak at $Q_3=0.24$ nm^{-1} and an inflection point around 0.3 nm^{-1}. The total structure factors $S(Q,\alpha)$ for a given orientation are accessible from the corresponding angle sectors according to Eq. (4) i.e., by dividing the measured intensities $I^{\pm}(Q,\alpha)$ by those calculated using the structure data as obtained from a fit at high-Q values, where $S(Q,\alpha)=1$. We note that using the two curves I^+ and I^- allows us to distinguish more reliably between the modulations resulting from the structure factor and those from the form factors. On the other hand, for the sectors with $\alpha=30°$, 60°, and 90°, it is more convenient to use the difference pattern I^+-I^- for the evaluation of $S(Q,\alpha)$ which scale at high Q according to the $\sin^2\alpha$ factor of Eq. (5b) [29]. The resulting structure factors $S(Q,\alpha)$ are plotted in Fig. 4 for the four sectors. The position of the observed peaks clearly suggests a hexagonal arrangement of the particles in planes aligned along the magnetic field. The peaks at Q_1 are identified as reflections of a hexagonal lattice with the Miller's indices (100), (−100), (010), (0−10), while Q_2 corresponds to the reflections (110) and (−1 −10). The observed ratio of $Q_2/Q_1=1.73$ corresponds precisely to $\sqrt{3}$ as expected for hexagonal symmetry. The basal plane must be oriented perpendicular to the direction of the incoming neutrons with the [110] direction aligned preferentially along the magnetic field. The magnetic moments of the particles are aligned along H. For the hexagonal symmetry two additional reflections (1−10) and (−110) at Q_1 are expected to appear in the vertical direction. The inflection

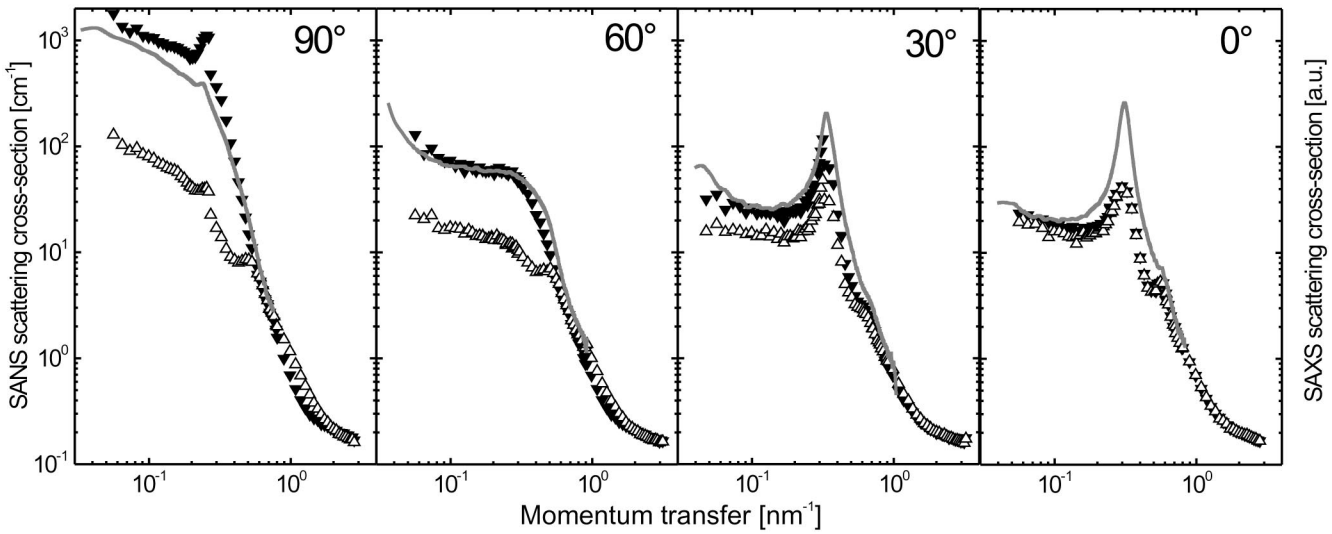

FIG. 3. (Color online) SANSPOL intensities I^+ (solid symbols) and I^- (open symbols) compared to SAXS results for the Co 3 vol % sample averaged over azimuth angles of 10° and 15° for SAXS, respectively, with sector centers at 90° ($\perp H$), 60°, 30°, and 0° ($\| H$). The magnetic field of 1 T (0.3 T) was applied perpendicular to the incident neutron beam. Note the perfect agreement in the peak positions and the shape of the curves in both techniques.

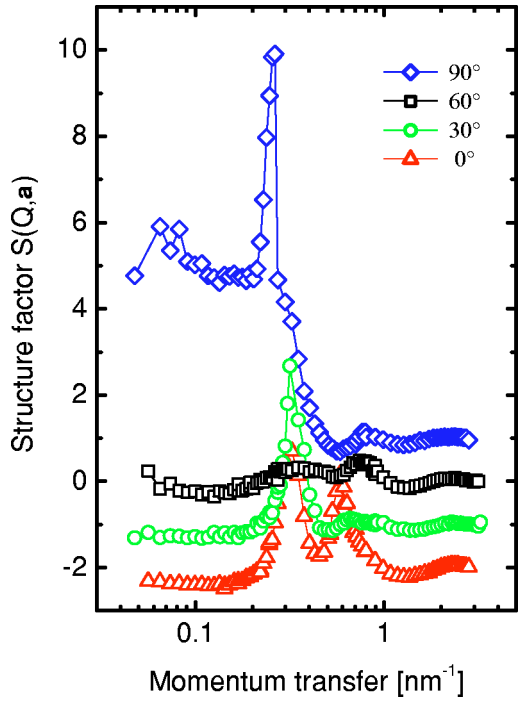

FIG. 4. (Color online) Anisotropic structure factors for Co 3% FF for H perpendicular to the incident neutrons for the sectors with $\alpha = 0°$ (1), 30° (2), 60° (3), and 90° (4) (ordinates for $\alpha = 60°$, 30°, and 0° were shifted by -1, -2, and -3 units, respectively). Pseudocrystalline texture peaks corresponding to Q_1 occur in sectors at 30° and 90°, for Q_2 in sector at 0°, and Q_3 in 90° only. Residual diffuse intensity observed in the sector of 0° at $Q_x = 0.29$ nm^{-1} results from chain segments aligned parallel to the magnetic field.

point observed in the 90° sector around $Q = 0.3$ nm^{-1} indicates effectively the presence of these peaks which are masked by a strong reflection at $Q_3 = 0.24$ nm^{-1}. In fact, the peaks observed at Q_3 can be assigned to a second type of preferred orientation which is present simultaneously with that defined by the reflections at Q_1 and Q_2: Particles are still arranged in hexagonal planes with the [110] orientation parallel to H, but the planes must be aligned parallel to the neutron beam, i.e., with [001] direction vertically. For this second type of texture, we expect then (001) and $(00-1)$ reflections to appear in the detector plane vertically and (110) and $(-1-10)$ reflections horizontally, while all reflections at Q_1 are out of the detector plane. The observed 2D pattern is in fact a superposition of both textures where the (110) reflections at Q_2 occur at the same position. The particle arrangement in both textures is represented in Fig. 5, together with the reciprocal lattice points observed in the detector plane. Both textures are fully equivalent and should be equally probable. However, the large difference between the intensities of the reflections Q_3 and Q_1, Q_2 shows that type II texture seems to be favored in the present case. When the samples are rotated around the vertical axis in the horizontal field by $\pm 25°$, no change of the peak position is detected. This shows that the hexagonal particle arrangement is fixed to the actual direction of the magnetic field. It is instructive to note that $S(Q, \alpha < 90°)$ is always lower than unity below Q_1, which is characteristic for the excluded volume effect. However, for the sector at $\alpha = 90°$ we observe $S(Q, \alpha = 90°) > 1$ which increases below Q_3 roughly with Q^{-1} (see also Fig. 3, sector $\alpha = 90°$). Such a Q dependence is characteristic for the scattering of cylindrical objects [31] where the long axis is perpendicular to the incident neutrons and perpendicular to the scattering vector **Q**. In addition, diffuse residual intensities are observed in planes perpendicular to the magnetic field at $Q_x = 0$ and $Q_x = \pm 0.29$ nm^{-1} (clearly

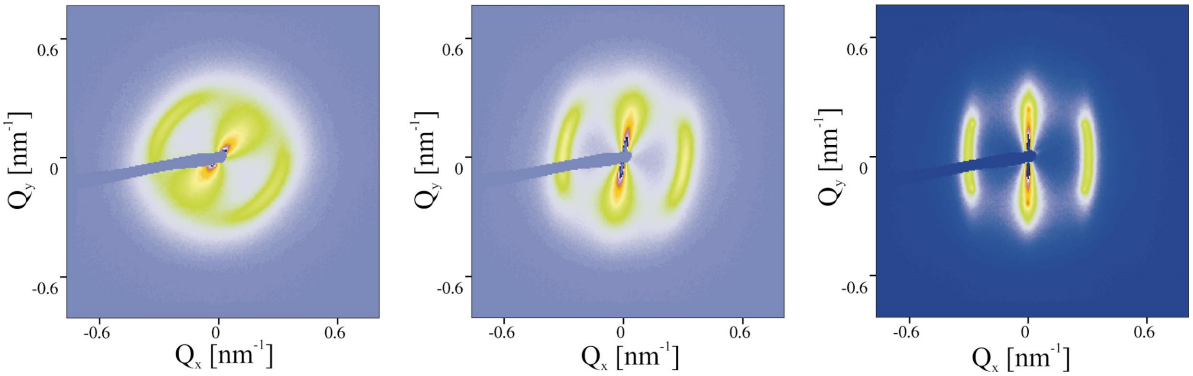

FIG. 5. (Color) Schematic representation of particle arrangements in hexagonal symmetry in textures of type I (top) and type II (bottom), and the corresponding reciprocal lattice points observed in the detector plane. The horizontal magnetic field is perpendicular to the incident beam.

visible for Co 1% in Fig. 1, in $I(-)$ of Fig. 2, and in the sector with $\alpha=0°$ of Fig. 4) which strongly indicates the presence of chainlike aggregates of particles. The magnetic dipoles of these particles are arranged in the attractive head-to-tail configuration which are aligned along the magnetic field. The nearest-neighbor distance inside the chains is estimated from $a=2\pi/Q_x$ to $a=21.5$ nm.

SANS and SANSPOL results are fully confirmed by a small-angle synchrotron x-ray scattering study performed on the same samples (DS1-DS6). The experiment is described in detail elsewhere [32]. As a typical example, we present 2D patterns of the 3 vol % DS3 sample in Fig. 6 measured in a horizontal magnetic field of 0.0 T, 0.065 T, and 0.53 T, applied perpendicular to the incident beam. Due to the high spatial resolution of the synchrotron instrument, we observe the setup of narrow peaks with increasing field and which disappear when the field is switched off. As with the neutrons, four well-resolved peaks correspond to the hexagonal in-plane reflections at Q_1 of type I texture and two reflections in vertical direction to type II. The cut along the vertical direction, plotted in Fig. 7, shows clearly the strong peak at Q_3, as well as a shoulder corresponding to a scattering vector Q_1. SAXS intensities averaged over azimuth angles of 15° in the four sectors are included in Fig. 3. We note the perfect agreement in the peak positions and the shape of the curves in both techniques. Below Q_3 the intensity in the sector with $\alpha=90°$ is found to increase continuously according to Q^{-1}, which confirms the presence of chain segments aligned along H. Since for x rays no orientation-dependent magnetic contribution is superimposed, all six {100} peaks are expected with equal intensities, which is effectively observed. The position of the SAXS peak at $Q_1=0.324$ nm^{-1} was found to be nearly independent of the concentration, while the peak width decreases and the position for Q_3 varies from 0.22 to 0.27 nm^{-1} in the concentration range between 2 vol % and 6 vol %.

In the whole series of concentration above 1 vol %, there are highly ordered regions of particles arranged with a hexagonal symmetry with a particular preferential orientation of [110] along the magnetic field, which give rise to these two kinds of textures. The actual values of Q_1 and Q_2 were found to be nearly independent of the concentration at $H=1$ T. The peak positions corresponding to Q_1 and Q_2 do not change significantly with the strength of the applied field. The corresponding hexagonal ''lattice constant'' is calculated from $Q(hk)=2\pi\sqrt{4(h^2+k^2+hk)/3a^2}$, leading to

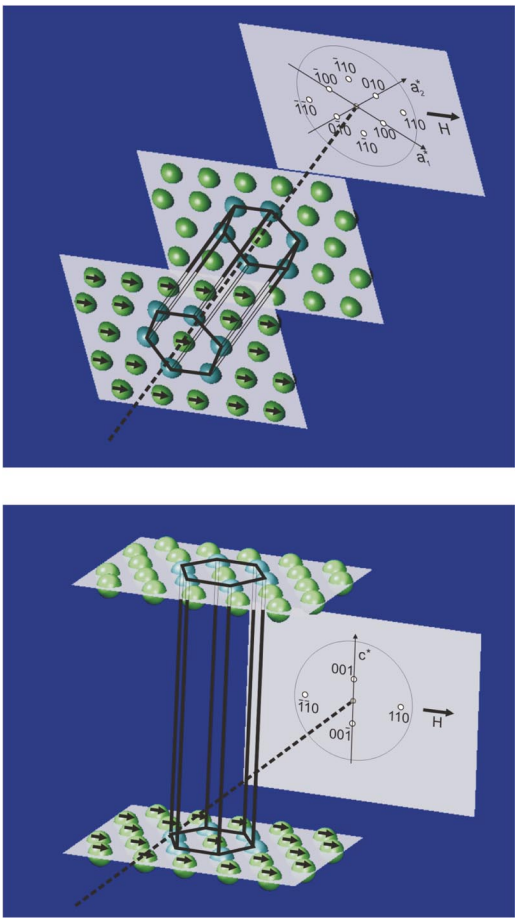

FIG. 6. (Color) SAXS pattern of 3 vol % Co in a horizontal magnetic field of 0.0 T (left), 0.065 T (center), and 0.57 T (right), applied perpendicular to the photon beam which shows the setup of the pseudocrystalline texture with increasing field. When the field is switched off, the texture relaxes back to full disorder. The sample tube axis formed an angle of about 35° with the field direction.

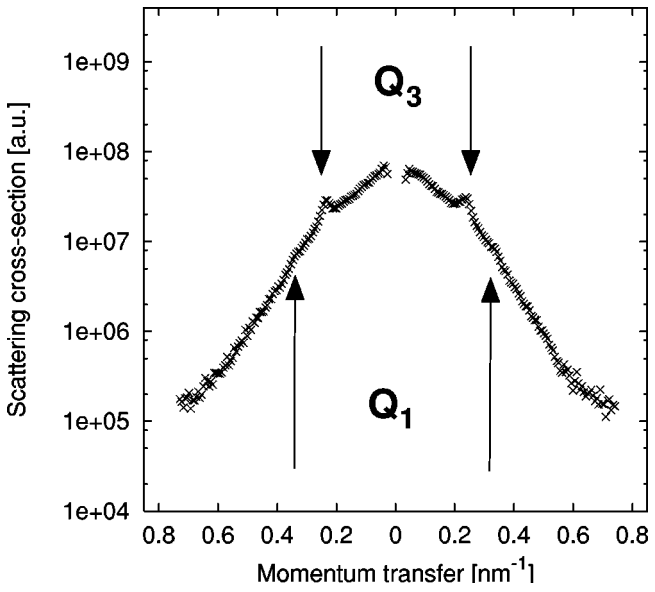

FIG. 7. Slice of Fig. 6 at 0.57 T along 0° reveals clearly the shoulder corresponding to hexagonal in-plane peaks at Q_1 beside the peak at Q_3 of texture II and the Q^{-1} behavior at low Q, corresponding to the particle chaining.

$a_{hex}=21.34$ nm. The average distance of particles in the basal plane therefore is found to be independent of the concentration and similar to that in the chain segments. From Q_3 we estimate the ''lattice constant'' in c-direction to $c=(2\pi/Q_3)$, which varies between 23 nm and 31 nm in the DS2 to DS6 samples. The fact that only one peak centered around Q_1 had been observed before in the structure factor of the D5 sample must be ascribed to a less pronounced ordering in this sample in textures of type I, resulting from a broader size distribution of the particles and to a larger interplane distance c (see below).

The structural arrangement perpendicular to the basal planes has been investigated on two samples D3a and D5a in a horizontal cryomagnet where the field up to 4 T was aligned parallel to the incoming neutrons. In this configuration, Q is always perpendicular to the moment direction. Since $\sin^2\alpha$ is unity for all values of Q, fully isotropic patterns are expected from Eq. (4) for SANS and SANSPOL as long as $S(Q,\alpha=90°)$ is isotropic. In the present case, stacking of the planes in both textures should be observable. In Fig. 8(a), the SANS pattern of the D3a (3%) sample averaged in sectors of 10° width are plotted for the sectors with $\phi=0°$ and 90°, respectively. When the magnetic field is switched to 1 T, a diffuse ring is observed at $Q_3=0.08-0.1$ nm^{-1} for D3a (3%), which is assigned to the (001) ''powder'' reflection. The maximum of the diffuse intensity is slightly enhanced in vertical direction $\phi=90°$ with respect to $\phi=0°$, which proves the presence of some texture with a slight preference of type II. The radial averaged SANSPOL intensities, shown in Fig. 8(b), confirmed these results. No further peak is detected, indicating that the correlations perpendicular to the magnetic field are less pronounced, i.e., the stacking of hexagonal planes is less well established in this sample.

In Co 5 vol % D5a sample, the diffuse peak appeared at $Q_3=0.21-0.23$ nm^{-1}. The large difference between 3% and 5% samples indicates effectively that with increasing particle concentration the average distance between hexagonal layers decreases from c(D3a)$=78$ nm to c(D5a) $=31$ nm in 5% sample, which is much larger than the (concentration independent) in-plane distance of $a_{hex}=21.34$ nm. The discrepancy in the layer spacing c between the DS3 and D3a samples is attributed to a much lower effective concentration (of about 2.1% from data fitting and from magnetic measurements) and to the larger size of the particles with average radius $R_c+d=7.2$ nm of the D3a sample.

The observed well-defined Bragg peaks clearly indicate that particles are aligned in an external magnetic field in pseudocrystalline ordered domains of hexagonal symmetry. The size of these domains can be estimated from the width of

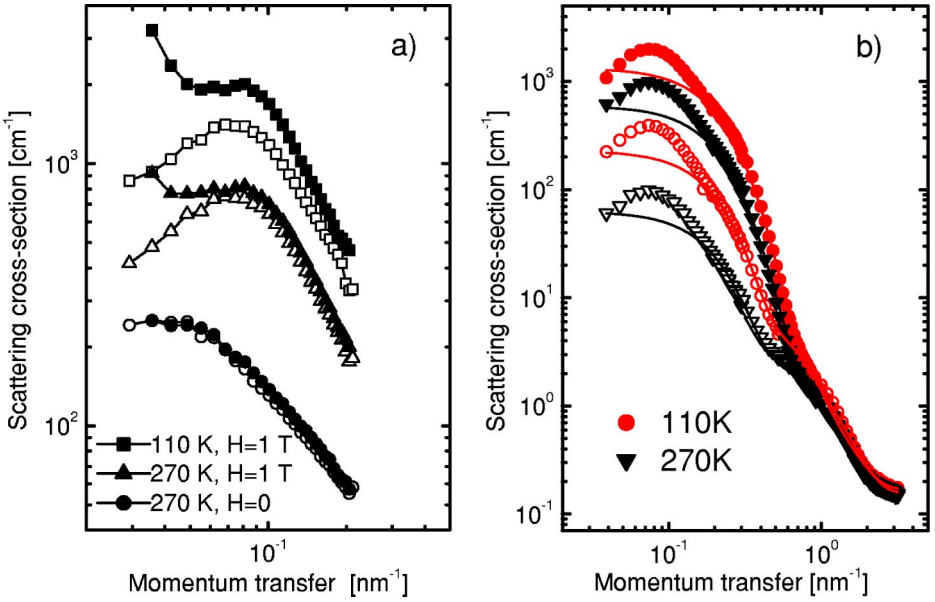

FIG. 8. (Color online) Temperature variation of the cross sections of 3 vol % Co-FF D3a sample in a magnetic field applied parallel to the incident neutrons. (a) The SANS signals at $H=0$ and $H=1$ T, averaged over sectors of 10° in horizontal (open symbols) and vertical directions (solid symbols), reveal the onset of field-induced correlations and some preferred orientation in texture of type II. (b) Radial averaged SANSPOL intensities I^+ and I^- at 270 K and 110 K measured at $H=0.3$ T. The solid lines represent the high-Q fit corresponding to noninteracting core-shell particles.

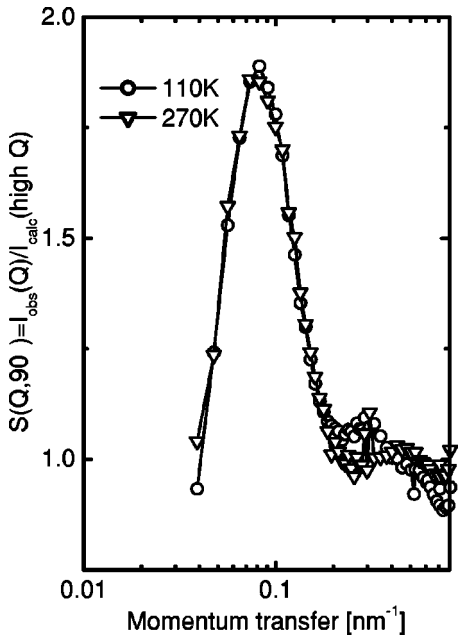

FIG. 9. Structure factor $S(Q,\alpha=90°)$ of the sample D3a at 280 K and 110 K as derived from Fig. 8(b).

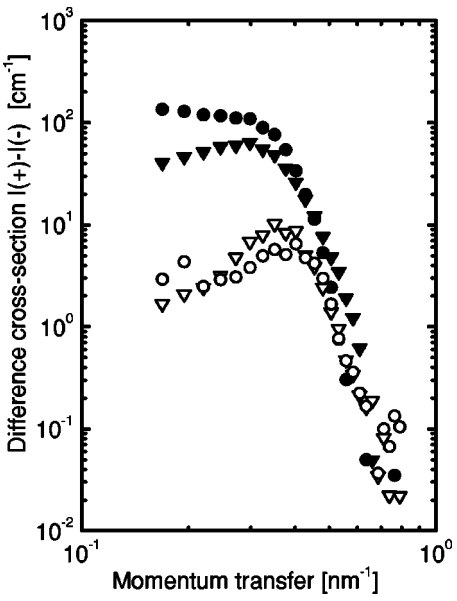

FIG. 10. Differences of the SANSPOL intensities I^+-I^- for DS2 sample (2 vol %) measured at $H=1$ T applied perpendicular to the incident neutrons in the liquid state (280 K; triangles) and in the solid state below the freezing temperature (30 K; circles). Two sectors are plotted at $\alpha=90°$ (solid symbols) and 30°(open symbols), where the peaks at Q_3 and Q_1 appear.

the peaks in Figs. 3, 4, and 9. Comparing the SANS and SAXS data (Fig. 3), very similar values of the full width at half maximum (FWHM) are observed despite the very different instrumental resolution of both techniques (which, for SAXS is by two orders of magnitude smaller than in SANS). The line broadening must therefore be largely dominated by the finite size of the ordered domains. When the instrumental resolution is neglected from the actual value of FWHM ($\Delta Q \approx 0.07$ nm^{-1}), we can estimate a lower limit for the correlation length $\xi = 2\pi/\Delta Q \approx 90$ nm.

B. Temperature dependence

When the D3a sample was cooled in an external field of 1 T, applied parallel to the incident neutrons, the total scattering intensity at first increased continuously and showed an abrupt jump between 190 and 170 K, below which it remained constant. The process was found to be fully reversible, i.e., heating up to 300 K recovered exactly the original scattering pattern. The jump around $T_f = 185$ K indicates freezing of the matrix. The SANS curves as shown in Fig. 8(a) for horizontal and vertical directions reflect an increase of the anisotropy (i.e., increasing texture), while the position of the maximum remains nearly unchanged at the freezing temperature. A quantitative evaluation of the SANPOL data was performed using the structural model derived for the diluted Co-FF. The fitted curves plotted in Fig. 8(b) as solid lines show the perfect agreement with the experimental data at high Q. The actual values of number density $N_p(T)$ and contrasts $\Delta\eta$ between matrix and shell are strongly temperature dependent due to the high thermal expansion coefficient of toluene as carrier liquid. N_p was found to increase by 18% and $\Delta\eta$ by 30% between 280 K and 110 K, which is in good agreement with the density variation of the solvent in liquid and solid states. The structure factor $S(Q,\alpha=90°)$ is now derived by dividing the experimental curves I^+ and I^- by the corresponding functions calculated with the parameters as obtained from the model fits in the high Q. By this analysis the same structure factor was obtained from I^+ and I^-, which showed that $S(Q,\alpha)$ is really independent of the neutron polarization, as implicitly assumed in Eq. (4). The resulting $S(Q,\alpha=90°)$, shown in Fig. 9, is found to be almost unchanged between 270 K and 110 K. Again, from the FWHM of the peak in Fig. 9, we derive a correlation length of the order of 90 nm. When $S(Q,\alpha=90°)$ as obtained from Fig. 9 (D3a sample) is compared to that of Fig. 4 (DS3 sample), beside the sample specific difference in the peak intensities and positions of Q_3, we note the absence of the Q^{-1} tail in Fig. 9, where $S(Q)<1$ for $Q<Q_3$. In fact, when the presumed chain segments are aligned parallel to the incident neutrons ($\|H$), the scattering contribution from the long axis of cylindrical objects must be absent in this scattering geometry. The freezing transition was followed on the 2 vol % DS2 sample when the magnetic field was applied perpendicular to the incident neutrons. The evolution is best seen in the nuclear-magnetic cross terms since all nonmagnetic contributions are totally eliminated. The differences I^+-I^- plotted in Fig. 10 for the sectors at 90° and 30° reveal again maxima at $Q_3 = 0.27$ nm^{-1} and $Q_1 = 0.34$ nm^{-1}, respectively. It turned out that the positions of the peaks were not changed significantly at the freezing transition but the intensity of the Q_3 peak (type II texture) increased at the expense of the Q_1 peak corresponding to the type I texture. An additional contribution with the characteristic Q^{-1} dependency occurs below $T_f = 185$ K, which implies in fact the freezing-in of uncorrelated chains aligned along the magnetic field.

C. Texture in zero field in confined geometries

An interesting effect is observed when the samples are measured in thin tubes at different orientations. Then even in ''zero field'' the $2d$ patterns are anisotropic, showing a marked increase of the intensity perpendicular to the axis of the tube. In the SAXS experiment (Fig. 6), the tube axis was oriented at about 35° to the horizontal direction. When the strength of the magnetic field applied horizontally is increased, the anisotropy moves gradually from the direction perpendicular to the tube axis towards the final direction of 90°, when the ''crystalline'' peaks are fully established. The anisotropy relaxes back to the original direction when the field is switched off. This anisotropy indicates some spontaneous formation of chain segments aligned along the tube axis. This could result from interactions of particles with the quartz-glass container walls.

In this confined geometry, the texture of type II seems to be favored, which leads to a dominating peak intensity at Q_3 in the vertical direction. This is in agreement with the SAXS data, where the Q_3 peak is well established and where the length of the vector depends again on the concentration.

V. SUMMARY

Field-induced interparticle correlations in concentrated surfactant stabilized Co ferrofluids have been studied by combining SANS, SANSPOL, and synchrotron SAXS. Samples of different particle concentrations of up to 6 vol % Co have been investigated in external magnetic fields applied parallel and perpendicular to the incident neutron or photon beam. Above 1 vol % Co, interparticle interactions are induced by an applied external magnetic field that gives rise to pseudocrystalline ordering of cobalt core-shell particles. The particles are arranged in hexagonal planes, with the magnetic moments parallel to the [110] direction. Two types of equivalent textures were found to be present simultaneously, corresponding to a stacking of the hexagonal planes in the horizontal or vertical direction. The average correlation length in the field-induced ordered domains corresponds to about 90 nm. The in-plane nearest-neighbor distance of $a_{hex} = 21.9$ nm is almost independent of the concentration and temperatures, whereas the distance between the neighboring planes, c, strongly varies from sample to sample between $c = 70$ nm and 25 nm. The ordering follows the direction of the applied field, i.e., the magnetic moments and the [110] directions are always aligned along the magnetic field. At least for applied fields >0.2 T, no change of the peak positions has been observed. In addition, segments of uncorrelated chains where the particle moments are arranged in the attractive head-to-tail conformation and aligned along the magnetic field were found to be present and frozen-in when the carrier liquid is solidified. The Q^{-1} behavior observed at low scattering vectors in the direction perpendicular to the magnetic field agrees well with Monte Carlo simulations [16] of the structure factors.

The pseudocrystalline lamellar hexagonal particle arrangement has never been observed experimentally before in magnetic colloids. Instead, isotropic liquidlike structure factors have been reported in γ-Fe_2O_3 citrate FF with some kind of a vitreous transition when at very high volume fractions the dipolar interaction parameter was of the order of $\gamma = 0.4$ [33]. When $S(Q)$ was interpreted as an isotropic liquidlike structure factor, the maximum observed at Q_1 was attributed to an average nearest-neighbor distance of $d(\mathrm{liq}) = (2\pi/Q_1) = 18.4$ nm, which is considerably shorter than that in the hexagonal layer ($a_{hex} = 21.9$ nm). In fact, a_{hex} is much larger than the composite particle diameter $\sigma = 2(R_c + d)$, which ranges between 11.9 nm (in samples of series DS) and 14.8 nm (in D3a, D5a) and exceeds even the hydrodynamic diameter of the particle as experienced from field-induced magnetoviscous damping [34].

On the other hand, recent computer simulations and theoretical work on electric dipolar systems revealed long-range ferroelectric orientational order without positional order where hexagonal, fcc, and bct structures have been found [35]. Modeling of competing repulsive and attractive interactions by rescaled mean sphere approximation always favors the formation of chains or chain segments at least for small values of γ [36]. Such spontaneous chaining in zero field has recently been observed by high-resolution cryogenic electron microscopy [37]. However, interactions between fluctuating parallel dipolar chains which are aligned in a magnetic field can lead to attractions perpendicular to the field direction. This lateral attraction could in fact give rise to the observed lamellar structures. Effectively, molecular dynamics studies performed by Hess [38,39] have predicted anisotropic structure factors when dipolar interaction exceeds the excluded volume effect. Above a critical value of the magnetic dipole moment a transition from the uniaxial to a lamellar, symmetry-breaking ordering should occur with almost close-packed in-plane structures. The results presented here confirm experimentally the transition from field-induced chainlike to lamellar ordering.

Simulations are currently performed in order to model the observed hexagonal ordering for the present case of Co ferrofluids, where the actual parameters of $\langle R_c \rangle = 3.6 - 5.4$ nm, $d = 2$ nm, and $M_{sat} = 1450$ kA/m correspond to interaction constant γ ranging from values between 1.4 and 8.

ACKNOWLEDGMENTS

Ferrofluid samples were provided by Dr. G. Gansau and Dr. N. Buske, Berlin Heart AG, Germany. Fruitful discussions with Professor D. Hohlwein, Professor S. Hess, Dr. P. Ilg, Dr. M. Kröger, and Dr. A. Heinemann are kindly acknowledged. The work was supported by the Priority program of the German Research Foundation (DFG Project No. WI-1151).

[1] E. Blums, A. Cebers, and M. M. Majorov, *Magnetic Fluids* (de Gruyter, New York, 1997).
[2] *Magnetically Controllable Fluids and Their Applications*, edited by S. Odenbach, Lecture Notes in Physics, Vol. 594 (Springer, Berlin, 2002).
[3] C. Alexiou *et al.*, JMMM **225**, 187 (2001).
[4] A. Wiedenmann, Mater. Sci. Forum **312-314**, 315 (1999).
[5] T. Keller, T. Krist, A. Danzig, U. Keiderling, F. Mezei, and A. Wiedenmann, J. Nucl. Instruments A **451**, 474 (2000).
[6] A. Wiedenmann, J. Appl. Crystallogr. **33**, 428 (2000).
[7] A. Wiedenmann, Physica B **297**, 226 (2001).
[8] A. Wiedenmann, Magnetohydrodynamics **37**, 236 (2001).
[9] A. Wiedenmann, A. Hoell, and M. Kammel, JMMM **252**, 83 (2002).
[10] M. Kammel, A. Hoell, and A. Wiedenmann, Scr. Mater. **44**, 2341 (2001).
[11] M. Kammel, A. Wiedenmann, and A. Hoell, JMMM **252**, 89 (2002).
[12] A. Hoell, R. Müller, A. Wiedenmann, and W. Gawalek, JMMM **252**, 92 (2002).
[13] P. de Gennes and P. Pincus, J. Phys.: Condens. Matter **11**, 189 (1970).
[14] A. Skjeltorp, J. Appl. Phys. **57**, 3285 (1985).
[15] J. Liu, E. Lawrence, A. Wu, M. Ivey, G. Flores, K. Javier, J. Bibette, and J. Richards, Phys. Rev. Lett. **74**, 2828 (1995).
[16] P. Camp and G. Patey, Phys. Rev. E **62**, 5403 (2000).
[17] S. Hess, J. Hayter, and R. Pynn, Mol. Phys. **53**, 1527 (1984).
[18] F. Gazeau, E. Dubois, J.-C. Bacri, F. Boué, A. Cebers, and R. Perzynski, Phys. Rev. E **65**, 031403 (2002).
[19] G. Kostorz, *Treatise on Material Science and Technology* (Academic Press, New York, 1978), Vol. 15.
[20] J. Percus and G. Yevick, Phys. Rev. **110**, 1 (1959).
[21] J. Brunner-Popela and O. Glatter, J. Appl. Crystallogr. **30**, 431 (1997).
[22] J. Pedersen, J. Appl. Crystallogr. **27**, 595 (1994).
[23] R. Moon, T. Riste, and W. Koehler, Phys. Rev. **181**, 920 (1969).
[24] R. Pynn, J. Hayter, and S.W. Charles, Phys. Rev. Lett. **51**, 710 (1983).
[25] J. Kohlbrecher, A. Wiedenmann, and H. Wollenberger, Z. Phys. **104**, 1 (1997).
[26] A. Wiedenmann, *Magnetically Controllable Fluids and Their Applications*, Lecture Notes in Physics, Vol. 594 (Springer, Berlin 2002), pp. 33–58.
[27] E. Papirer, P. Horny, and H. Ballard, J. Colloid Interface Sci. **94**, 220 (1983).
[28] N. Buske, DE Patent No. 197 58 350 (1997).
[29] A. Heinemann and A. Wiedenmann, J. Appl. Crystallogr. **36**, 845 (2003).
[30] D. Tatchev, A. Heinemann, A. Hoell, and A. Wiedenmann (to be published).
[31] O. Glatter and O. Kratky, *Small Angle X-ray Scattering* (Academic Press, London, 1982).
[32] A. Hoell, P. Boesecke, M. Kammel, and A. Wiedenmann (unpublished).
[33] F. Cousin and V. Cabuil, Prog. Colloid Polym. Sci. **115**, 77 (2000).
[34] J. Embs *et al.*, Phys. Rev. E (to be published).
[35] B. Groh and S. Dietrich, Phys. Rev. E **63**, 021203 (2001).
[36] J. Hayter, J. Appl. Crystallogr. **21**, 737 (1988).
[37] K. Butter, P. Bomans, P. Frederik, G. Vroege, and A. Philipse (unpublished).
[38] S. Hess, in *Physics of Complex and Supramolecular Fluids*, edited by S. A. Safran and N. A. Clark (Wiley Interscience, New York, 1987), pp. 631–642.
[39] S. Hess, T. Wieder, and M. Kröger, Magnetohydrodynamics **37**, 297 (2001).